

Buckling of scroll waves

Hans Dierckx, Henri Verschelde

*Department of Mathematical Physics and Astronomy,
Ghent University, Krijgslaan 281, 9000 Ghent, Belgium*

Özgür Selsil, Vadim Biktashev

Department of Mathematical Sciences, University of Liverpool, Liverpool L69 7ZL, UK

(Dated: May 25, 2019)

A scroll wave in a thin layer of an excitable medium with negative filament tension will have a tendency to deform into a buckled, precessing state. Experimentally this will be seen as meandering of the spiral wave on the surface, the amplitude of which grows with the thickness of the layer, until a break-up to scroll wave turbulence happens. We present a theory for this phenomenon and illustrate it with numerical examples.

PACS numbers: 05.45.-a, 87.23.Cc, 82.40.Ck, 91.30.Ab

Spiral waves in two-dimensions, and scroll waves in three-dimensions, are regimes of self-organization observed in physical, chemical and biological dissipative systems, where wave propagation is supported by a source of energy stored in the medium [1–9]. Due to effective localization of the critical adjoint eigenfunctions, or “response functions” [10, 11], the dynamics of a spiral wave can be asymptotically described as that of pointwise objects, in terms of its instant rotation centre and phase [12]. The third dimension endows scrolls with extra degrees of freedom: the filaments, around which the scroll waves rotate, can bend, and the phase of rotation may vary along the filaments, giving scrolls a twist [13]. The localization of response functions allows description of scroll waves as string-like objects [10, 14–18]. One manifestation of the extra degrees of freedom is the possibility of “scroll wave turbulence” due to negative tension of filaments [19]. It has been speculated that this scroll wave turbulence is in some respects similar to the hydrodynamic turbulence, and may provide insights into the mechanisms of cardiac fibrillation [10, 19, 20].

The motivation for the present study comes from the analogy with hydrodynamic turbulence. As is well known, at intermediate Reynolds numbers, laminar flow can be unstable leading to non-stationary regimes which however are not yet turbulent [8]. The possibility of similar pre-turbulent regimes in scroll waves is interesting, e.g. in view of its possible relevance to cardiac arrhythmias. Cardiac muscle may be considered quasi-two-dimensional if it is very thin. Since scroll turbulence is essentially three-dimensional, it bears no reflection on behaviour of spiral waves in truly two-dimensional media. Hence the behaviour of scrolls in layers of a given thickness may be effectively two-dimensional, unaffected by the negative tension, or truly three-dimensional, with full blown turbulence, or an intermediate regime. So understanding of possible intermediate regimes is vitally important for interpretation of experimental data and for possible medical implications.

Here we consider one such intermediate regime, which is illustrated in fig. 1. This is a snapshot of a scroll wave

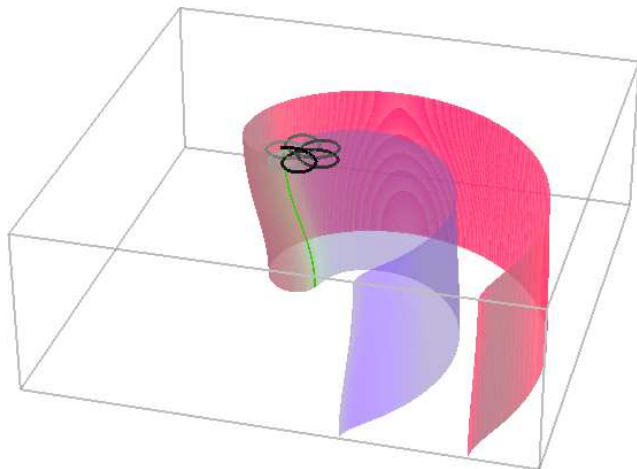


FIG. 1: (color online) Buckled scroll and filament, with the tip path on the top of the box. Parameters $a = 1.1$, $b = 0.19$, $c = 0.02$, $D_v = 0.10$, box size $20 \times 20 \times 6.9$ [21].

solution of an excitable reaction-diffusion model

$$\frac{\partial \mathbf{u}}{\partial t} = \mathbf{f}(\mathbf{u}) + \mathbf{D} \nabla^2 \mathbf{u}, \quad (1)$$

where $\mathbf{u}, \mathbf{f} \in \mathbb{R}^\ell$, $\mathbf{D} \in \mathbb{R}^{\ell \times \ell}$, $\mathbf{u}(\vec{r}, t)$ is the dynamic vector field, $\vec{r} \in \mathbb{R}^3$, \mathbf{D} is diffusion matrix and $\mathbf{f}(\mathbf{u})$ are reaction kinetics that sustain spiral wave formation, in a rectangular box $\vec{r} = (x, y, z) \in [0, L_x] \times [0, L_y] \times [0, L_z]$, with initial conditions in the form of a slightly perturbed straight scroll. In boxes with smaller L_z , the scrolls keep straight and rotate steadily. In large enough L_z , the standard scroll wave turbulence develops. In a range of L_z including $L_z = 6.9$ as in fig. 1, the straight scroll is unstable, and its filament, after an initial transient, assumes an S-like shape which remains constant and precesses with a constant angular velocity. In almost any $z = \text{const}$ section, including the upper and lower surfaces, one observes spiral waves with circular core, whose instant rotation centre, in turn, rotates with an angular speed which changes little with all L_z , but with a radius which is van-

ishingly small for $L_z \gtrsim L_*$ and growing with L_z . The resulting tip path, observed on the upper and lower surfaces, is similar to classical two-periodic meander [22].

The instability is akin to the Euler's buckling in elasticity, which is deflection of a straight beam under a sufficiently high compressive stress [23]. An analytical insight into scroll buckling can be via the asymptotic filament motion equations, considered to a sufficiently high order to take into account all relevant effects [17, 18]. These may be likened to the equations of an elastic beam; the difference to have in mind is that scroll rotates around the filament and the filament itself precesses, so we cannot talk about an equilibrium, but only about a relative equilibrium. Consider a generic reaction-diffusion system like (1), supporting steadily rotating spiral waves, in a spatial domain $(x, y, z) \in \mathbb{R} \times \mathbb{R} \times [0, L_z]$, i.e. we neglect the influence of the side walls. A simplified version of the filament equation of motion can be written as

$$\begin{aligned} (\dot{\vec{R}})_\perp = & \left(\gamma_1 + \gamma_2 \partial_\sigma \vec{R} \times \right) \partial_\sigma^2 \vec{R} - \left(g_1 + g_2 \partial_\sigma \vec{R} \times \right) (\partial_\sigma^4 \vec{R})_\perp \\ & + |\partial_\sigma^2 \vec{R}|^2 \left(b_1 + b_2 \partial_\sigma \vec{R} \times \right) \partial_\sigma^2 \vec{R} + \text{h.o.t.}, \end{aligned} \quad (2)$$

where $\vec{R}(\sigma, t)$ is filament position and σ is arclength. Derivation of the linearized version of this equation is given the Appendix [21]. This is in fact a low-twist limit of generic equations of motion; account of twist effects leads to qualitatively the same results, with a complicated combination of coefficients in place of b_1 and b_2 . The coefficients in (2) are defined via integrals involving the unperturbed spiral wave solution \mathbf{U} , its angular velocity ω_0 , the linearized operator $\hat{\mathbf{L}}$, the translational symmetry eigenmode \mathbf{V}_+ and the corresponding ‘‘response function’’ \mathbf{W}_+ , which is the adjoint eigenmode with respect to scalar product $\langle \mathbf{u} | \mathbf{v} \rangle \equiv \iint_{\mathbb{R}^2} \mathbf{u}^T \mathbf{v} \, dx \, dy$. The filament *tension*, with scalar γ_1 and pseudoscalar γ_2 components, is $\gamma_1 + i\gamma_2 = \langle \mathbf{W}^+ | \mathbf{D} | \mathbf{V}_+ \rangle$ as in [10, 16], and the filament *rigidity* is $g_1 + ig_2 = \langle \mathbf{W}^+ | \mathbf{D} (\hat{\mathbf{L}} - i\omega_0)^{-1} (\mathbf{1} - | \mathbf{V}_+ \rangle \langle \mathbf{W}^+ |) \mathbf{D} | \mathbf{V}_+ \rangle$. For our numerical examples, we have calculated these using `dxspiral` software [24] based on the method described in [25]. The expression for the *nonlinear tension* $b_1 + ib_2$ is noticeably more complicated and difficult to compute, and even more so with account of twist corrections; we did not attempt that and leave b_1 and b_2 as phenomenological parameters. By appropriately choosing the origin of the x and y coordinates, we look for solutions of (2) in the form $\vec{R} = X(z, t) \vec{e}_x + Y(z, t) \vec{e}_y + z \vec{e}_z$, for small $|X(z, t)|, |Y(z, t)|$. Boundary conditions $\partial_z \mathbf{u} = 0$ at $z = 0, L_z$ lead to $\partial_z X = \partial_z^3 X = \partial_z Y = \partial_z^3 Y = 0$ at $z = 0, L_z$. Linearized solutions will be superpositions of

$$X + iY = W(t) \cos(k_z z), \quad k_z = n\pi/L_z, \quad n \in \mathbb{Z}, \quad (3)$$

where the complex amplitude W evolves by

$$\dot{W} = \mu(k_z)W, \quad \mu(k_z) = -(\gamma_1 + i\gamma_2)k_z^2 - (g_1 + ig_2)k_z^4. \quad (4)$$

Hence the straight scroll solution $X = Y = 0$ is stable if $-\gamma_1 - g_1 k_z^2 > 0$ for any allowed wavenumber $k_z = n\pi/L_z$,

$n \in \mathbb{Z}_+$. In the case of negative filament tension $\gamma_1 < 0$, we have a finite range of unstable wavenumbers if also $g_1 > 0$. Then the stability is violated if $k_z < k_*$ where $k_* = (-\gamma_1/g_1)^{1/2}$, which happens first at $n = 1$, so $L_z > L_*$, where

$$L_* = \pi(-g_1/\gamma_1)^{1/2}. \quad (5)$$

The above theory works well if the Maclaurin expansion of $\mu(k_z)$ given by (4) approximates well for $k_z \in (0, k_*)$. This may be so e.g. if $|\gamma_1|$ is small. Further, the standard bifurcation analysis leads to solutions of the form

$$X + iY = A \cos(k_z z) e^{i\Omega t} + \mathcal{O}\left((L_z - L_*)^{3/2}\right), \quad (6)$$

where

$$\begin{aligned} A^2 = & \frac{16g_1(L_z - L_*)}{(-\gamma_1)B}, \quad B = 6b_1 - 4g_1, \quad (7) \\ \Omega = & \gamma_1(\gamma_2 g_1 - \gamma_1 g_2)/g_1^2 + \mathcal{O}(L_z - L_*), \end{aligned}$$

and the bifurcation is supercritical if $B > 0$.

So, in absence of other instabilities (say two- or three-dimensional meander), and subject to three inequalities $\gamma_1 < 0$, $g_1 > 0$, $B > 0$ and the limits of small $|\gamma_1|$ and small $L_z - L_*$, we have an approximate analytical solution (5)–(7). The condition of negative tension, $\gamma_1 < 0$, is the primary one and the key cause of the buckling instability. The condition of $g_1 > 0$ ensures that the fourth-order arclength derivative is sufficient to suppress high-wavenumber perturbations and is therefore only technical, i.e. important only for particular formulas but not the phenomenon itself. The condition $B > 0$ insures supercriticality; if it is violated, then the branch described by (5)–(7) appears for $L_z < L_*$ and is unstable. This condition however does not preclude this branch from becoming stable at larger A , so is moderately restrictive. Finally, the conditions $|\gamma_1| \ll 1$, $|L_* - L_z| \ll 1$ are purely technical and only required for the asymptotics; in reality, one would expect some finite, inter-dependent ranges for γ_1 and L_z to support buckled scrolls. Hence we expect that buckled scrolls are fairly typical and have ‘‘finite chances’’ to be observed in some range of L_z , if only $\gamma_1 < 0$.

We illustrate the above theory with numerical simulations [21] using reaction-diffusion system (1) with Barkley [26] kinetics, $\ell = 2$, $\mathbf{u} = (u, v)$, $\mathbf{f} = (f, g)^T$, $f = c^{-1}u(1-u)(u - (v+b)/a)$, $g = u - v$, and $\mathbf{D} = \text{diag}(1, D_v)$. We mostly use kinetic parameters a, b, c as in [27], which give negative filament tension $\gamma_1 < 0$, and consider also $D_v > 0$ so as to make $|\gamma_1|$ smaller; note that for $D_v = 1$, we are guaranteed that $\gamma_1 = 1 > 0$.

Fig. 2 illustrates dependence of the buckling amplitude and precession frequency on the thickness of the layer, L_z , for the same set of parameters as used to generate fig. 1. We see from panel (a) that just above the bifurcation point, $L_z \gtrsim L_*$, there is good agreement with (7). Linear fitting of the $A^2(L_z)$ dependence for the weakest buckled scrolls gives bifurcation point $L_* \approx 6.310$, and

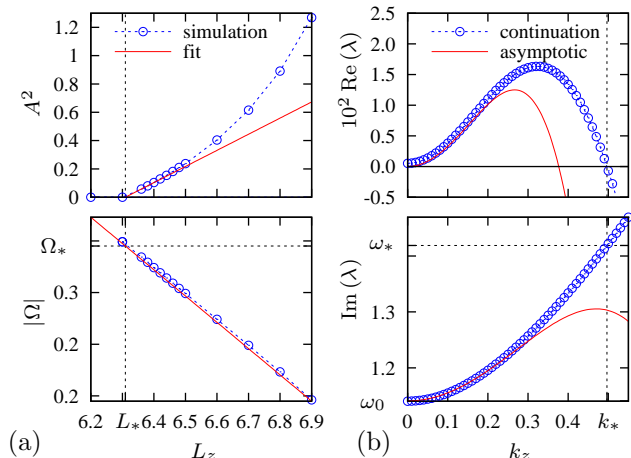


FIG. 2: (color online) (a) Bifurcation diagram ($a = 1.1$, $b = 0.19$, $c = 0.02$, $D_v = 0.1$): the amplitude (upper panel) and precessing frequency (lower panel) of the straight and buckled scrolls. (b) The corresponding translational branch: real part (upper panel) and imaginary part (lower panel).

a linear extrapolation of the precessing frequency from the same set gives $\Omega(L_*) \approx 0.2789$. Panel (b) shows the results of the linear analysis, both asymptotic as given by (4) and obtained by numerically solving the eigenvalue problem

$$(\hat{\mathbf{L}} - k_z^2 \mathbf{D})\mathbf{v}_{k_z} = \lambda(k_z)\mathbf{v}_{k_z}, \quad (8)$$

while varying k_z , as in [28]. The latter gives the $k_* \approx 0.497$, i.e. $L_* = \pi/k_* \approx 6.33$, in agreement with the direct simulations shown in panel (a). The `dxspiral` calculations using (5) give $\gamma_1 = -0.353$, $g_1 \approx 2.49$, resulting in $k_* \approx 0.376$. The nearly 25% difference between the continuation and asymptotic predictions is consistent with k_z being not very small, and should decrease for smaller $|\gamma_1|$. This is indeed true, as seen below. The precessing frequency predicted by continuation is $\Omega_* = \text{Im}(\lambda(k_*)) - \omega_0 \approx 1.4188 - 1.1408 = 0.2780$, again in agreement with simulations.

Fig. 3 illustrates variations in the buckling bifurcation caused by change of parameter D_v . Panels (a,b) present the case where the filament tension is strongly negative, for parameters as in [27]. The `dxspiral` predictions are $\gamma_1 \approx -2.18$, $g_1 \approx 48.2$ so the asymptotic $k_* \approx 0.213$ is vastly different from the continuation prediction $k_* \approx 0.890$, and this discrepancy is clearly visible in panel (b). Yet, panel (a) shows that the bifurcation still takes place, and the critical thickness $L_* \approx 3.60$ is in agreement with the prediction of the continuation, $L_* = \pi/k_* \approx 3.53$. This confirms that the assumption of smallness of the negative tension is only technical and does not preclude buckled scroll solutions, which still occur via a supercritical bifurcation as the medium thickness varies.

Panels (c,d) present a variation where the negative filament tension is much smaller ($D_v = 0.25$). Panel (d)

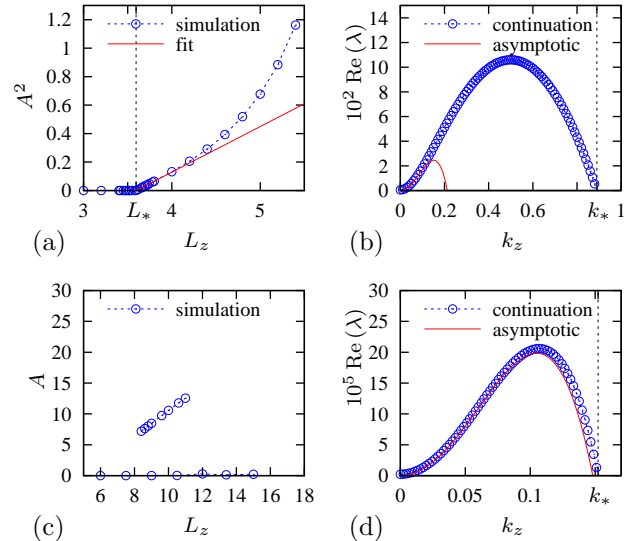


FIG. 3: (color online) (a) Bifurcation diagram (buckling amplitude) and (b) translational branch (real part), for $a = 1.1$, $b = 0.19$, $c = 0.02$, $D_v = 0$. (c,d) Same, for $a = 1.1$, $b = 0.19$, $c = 0.02$, $D_v = 0.25$.

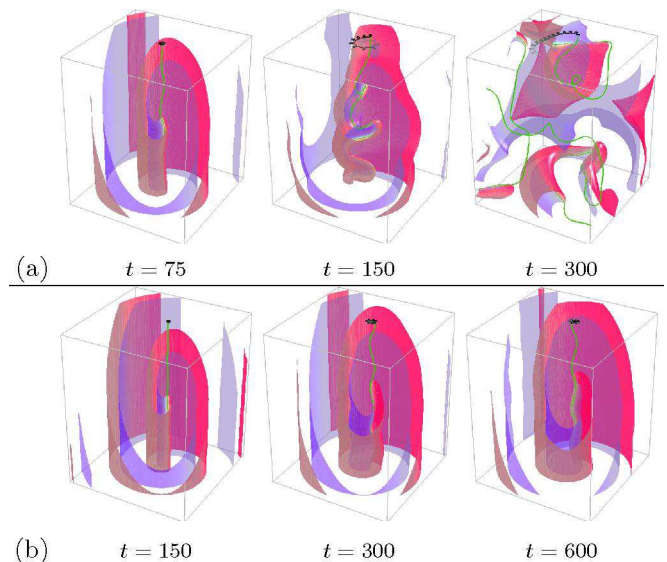


FIG. 4: (color online) Development of (a) autowave turbulence ($a = 1.1$, $b = 0.19$, $c = 0.02$, $D_v = 0$) and (b) “wrinkled scroll” as restabilized solution after 3D meandering bifurcation (same parameters except $b = 0.17$). Wavefronts are cut out by clipping planes halfway through the volume, to reveal the filaments.

shows much better agreement between the asymptotics: $\gamma_1 \approx -0.0362$, $g_1 \approx 1.65$, such that $k_* = 0.148$, whereas continuation gives $k_* = 0.152$. However, the bifurcation in this case is subcritical with a hysteresis, see panel (c), which indicates that the assumption of supercriticality is not absolute, and that a subcritical bifurcation can likewise lead to buckled scroll solutions.

Finally, we illustrate the difference of the buckling

bifurcation we have described here, from the “3D meander” bifurcation described previously by Henry and Hakim [28]. On the formal level, the restabilized scrolls following a 3D meandering instability look similar: at any moment, the filament has a flat sinusoidal shape (given Neumann boundary conditions), and the top and bottom surfaces show meandering spiral wave pictures. However the behaviour is completely different as L_z grows, as illustrated in fig. 4. Row (a) shows that in the negative tension case, at sufficiently large L_z the scroll buckles so much it breaks up and a scroll turbulence develops, in agreement with previous results. Row (b) shows that in case of 3D meander, the amplitude remains bounded, and even when L_z is large enough to hold several wavelengths of the curved filament, the restabilized “wrinkled scroll” can persist for a long time (compare these with “zigzag shaped filaments” described in [29]). Moreover, these two bifurcations occur in different parametric regions via different mechanisms.

To summarize, we predict that in an excitable medium

with negative nominal filament tension γ_1 , a thin quasi-two-dimensional layer of such medium can exhibit buckled scroll waves, with S-shaped filament which precesses while maintaining a constant shape. On the surface of the layer this will look like a classical flower-pattern meander, which emerges as the layer thickness L_z grows through the critical value L_* , via “transition to meander” similar to one described for 2D media [30, 31], with the difference that this happens purely due to change in L_z rather than change in reaction kinetics, and that the phase of the meander is opposite on the opposite surfaces of the layer. The knowledge about this phenomenon and its properties are important for planning and interpretation of experiments with layers of excitable media.

Acknowledgments Authors are grateful to I.V. Biktasheva for helpful discussions. The study was supported in part by EPSRC grant EP/D074789/1 and EP/I029664/1 (UK). H.D. acknowledges the FWO-Flanders for personal funding and providing computational infrastructure.

-
- [1] A. M. Zhabotinsky and A. N. Zaikin, in *Oscillatory processes in biological and chemical systems*, edited by E. E. Selkov, A. A. Zhabotinsky, and S. E. Shnol (Nauka, Pushchino, 1971), p. 279.
- [2] M. A. Allesie, F. I. M. Bonke, and F. J. G. Schopman, *Circ. Res.* **33**, 54 (1973).
- [3] F. Alcantara and M. Monk, *J. Gen. Microbiol.* **85**, 321 (1974).
- [4] N. A. Gorelova and J. Bures, *J. Neurobiol.* **14**, 353 (1983).
- [5] B. F. Madore and W. L. Freedman, *Am. Sci.* **75**, 252 (1987).
- [6] S. Jakubith, H. H. Rotermund, W. Engel, A. von Oertzen, and G. Ertl, *Phys. Rev. Lett.* **65**, 3013 (1990).
- [7] J. Lechleiter, S. Girard, E. Peralta, and D. Clapham, *Science* **252** (1991).
- [8] M. C. Cross and P. C. Hohenberg, *Rev. Mod. Phys.* **65**, 851 (1993).
- [9] T. Frisch, S. Rica, P. Coulet, and J. M. Gilli, *Phys. Rev. Lett.* **72**, 1471 (1994).
- [10] V. N. Biktashev, A. V. Holden, and H. Zhang, *Phil. Trans. Roy. Soc. Lond. ser. A* **347**, 611 (1994).
- [11] I. V. Biktasheva, Y. E. Elkin, and V. N. Biktashev, *Phys. Rev. E* **57**, 2656 (1998).
- [12] V. Biktashev and A. Holden, *Chaos, Solitons and Fractals* **5**, 575 (1995).
- [13] A. T. Winfree and S. H. Strogatz, *Physica D* **8**, 35 (1983), 9:65–80.
- [14] L. Yakushevich, *Studia Biophysica* **100**, 195 (1984).
- [15] P. K. Brazhnik, V. A. Davydov, V. S. Zykov, and A. S. Mikhailov, *Zh. Eksp. Teor. Fiz.* **93**, 1725 (1987).
- [16] J. Keener, *Physica D* **31**, 269 (1988).
- [17] H. Verschelde, H. Dierckx, and O. Bernus, *Phys. Rev. Lett.* **99**, 168104 (2007).
- [18] H. Dierckx, Ph.D. thesis, Ghent University (2010).
- [19] V. N. Biktashev, *Int. J. of Bifurcation and Chaos* **8**, 677 (1998).
- [20] A. T. Winfree, *Science* **266**, 1003 (1994).
- [21] See EPAPS Document No. [number will be inserted by publisher] for the Appendix with details of asymptotic and numerical procedures, and a movie. For more information on EPAPS, see <http://www.aip.org/pubservs/epaps.html>.
- [22] V. S. Zykov, *Biophysics* **31**, 940 (1986).
- [23] L. D. Landau and E. M. Livshitz, *Theory of Elasticity* (Pergamon, Oxford, 1975).
- [24] D. Barkley, V. N. Biktashev, I. V. Biktasheva, G. V. Boryugov, and A. J. Foulkes, *DXSpiral: a code for studying spiral waves on a disk*, <http://www.csc.liv.ac.uk/~ivb/software/DXSpiral.html>.
- [25] I. V. Biktasheva, D. Barkley, V. N. Biktashev, G. V. Boryugov, and A. J. Foulkes, *Phys. Rev. E* **79**, 056702 (2009).
- [26] D. Barkley, *Physica D* **49**, 61 (1991).
- [27] S. Alonso, R. Kahler, A. S. Mikhailov, and F. Sagues, *Phys. Rev. E* **70**, 056201 (2004).
- [28] H. Henry and V. Hakim, *Phys. Rev. E* **65**, 046235 (2002).
- [29] C. Luengviriyaya, U. Storb, G. Lindner, S. C. Müller, M. Bär, and M. J. B. Hauser, *Phys. Rev. Lett.* **100**, 148302 (2008).
- [30] D. Barkley, M. Kness, and L. S. Tuckerman, *Phys. Rev. A* **42**, 2489 (1990).
- [31] A. Karma, *Phys. Rev. Lett.* **65**, 2824 (1990).

Appendix to “Buckling of scroll waves ”
by H. Dierckx, H. Verschelde, Ö. Selsil and V.N. Biktashev

Direct numerical simulations

We used two schemes, an explicit and a semi-implicit.

a. Explicit scheme: Forward Euler in time with step Δ_t , and 7- or 19-point approximation of the Laplacian with step Δ_x in cuboid domains of size $L_x \times L_y \times L_z$. We used sequential solver EZSCROLL by Barkley and Doyle [1], and our own sequential and MPI-parallel solvers.

b. Semi-implicit: Operator splitting between reaction and diffusion substeps, with the diffusion substep by Brian’s three-dimensional alternating-direction procedure [2, 3] which is unconditionally stable and second-order time accurate, implemented in our own sequential solver.

The initial conditions were in the form of a straight scroll wave with the filament along the z coordinate, slightly perturbed: slightly twisted (z -dependent rotation) or slightly bended (z -dependent shift).

The details specific for different simulation series are listed in Table I. The bifurcation plots in figures 2(a) and 3(a) each were obtained through two series of simulations: one with fixed Δ_x and varied $N_z = L_z/\Delta_x$, and the other, to achieve a finer tuning of L_z , with fixed N_z and varied Δ_x .

Postprocessing

The results of simulations were visualized using a slightly modified graphical part of EZSCROLL, based on marching cubes algorithm [1]. Figures 1 and 4 show snapshots of surfaces $u(x, y, z, t) = u_*$ at selected moments of time, semi-transparent and coloured depending on corresponding values of $v(x, y, z, t)$: red for smaller v , blue for larger v , with a smooth transition at around $v = v_*$. The instant filament, or “tipline” was defined as intersection of isosurfaces $u(x, y, z, t) = u_*$ and $v(x, y, z, t) = v_*$, and is shown in green. The path of the end of the tip line at the upper surface, i.e. the curve defined by

TABLE I: Discretization parameters for direct numerical simulations. SI: semi-implicit; E7: explicit with 7-point Laplacian; E19: explicit with 19-point Laplacian.

Figure	Scheme	Δ_t	Δ_x	$L_x = L_y$	L_z
1	SI	1/60	1/10	20	6.9
2(a)	E7	$\Delta_x^2/12$	1/10	16	varied
2(a)	E7	$\Delta_x^2/12$	$L_z/64$	$160\Delta_x$	varied
3(a)	E19	$3\Delta_x^2/16$	1/5	17	varied
3(a)	E19	$3\Delta_x^2/16$	$L_z/19$	$85\Delta_x$	varied
3(c)	E7	$3\Delta_x^2/20$	1/5	120	varied
4	E7	$\Delta_x^2/12$	1/5	40	50

$u(x, y, L_z, t) = u_*$ and $v(x, y, L_z, t) = v_*$, is drawn in grayscale, with darker shade corresponding to more recent position. We made the traditional choice for Barkley kinetics, $u_* = 1/2$ and $v_* = a/2 - b$.

The buckling amplitude and precession were defined in two steps. Firstly, at a sufficiently frequent grid of time moment, say at least 30 per period, we approximated the simulation tip line, represented as functions $x = X(z, t)$, $y = Y(z, t)$, by

$$\begin{bmatrix} x \\ y \end{bmatrix} = \begin{bmatrix} A_x \\ A_y \end{bmatrix} (t) \cos(\pi z/L_z), \quad (9)$$

using least squares. The resulting raw buckling vector was then averaged through periods,

$$\left\langle \begin{bmatrix} A_x \\ A_y \end{bmatrix} \right\rangle \left(\frac{t_{j+1} + t_j}{2} \right) = \frac{1}{t_{j+1} - t_j} \int_{t_j}^{t_{j+1}} \begin{bmatrix} A_x \\ A_y \end{bmatrix} dt$$

where the periods were defined via u records at a selected point,

$$u(x_r, y_r, z_r, t_j) = u_*, \quad \partial_t u(x_r, y_r, z_r, t_j) > 0,$$

which was typically chosen in the box corner, $(x_r, y_r, z_r) = (0, 0, 0)$. These period-averaged data were then used to define amplitude $A = |\langle A_x \rangle + i \langle A_y \rangle|$ and phase $\Phi = \arg(\langle A_x \rangle + i \langle A_y \rangle)$ of buckling. The buckling was considered established when the graph of $A(t)$ showed saturation, subject to residual numerical noise. The value of $A(t)$ average over a sufficiently long “established interval” of time was then used for graphs in figures 2(a) (top) and 3(a). The buckling phase was made “continuous” (so the difference between consecutive readings of Φ does not exceed π) by transformation $\Phi(t) \mapsto \Phi(t) + 2\pi N_t$ with appropriately chosen $N_t \in \mathbb{Z}$. The resulting normalized dependence was approximated in the same established interval using least squares by a linear function of t , the slope of which gave the estimate of precession frequency Ω , used for figures 2(a) (bottom).

For fig. 3(c), the buckling was so strong that the filament shape was not approximated well by (9). There we took instead $A_x(t) = \frac{1}{2}(X(L_z, t) - X(0, t))$, $A_y(t) = \frac{1}{2}(Y(L_z, t) - Y(0, t))$ as the raw data.

Linearized theory

To derive the critical medium thickness for filament buckling, the Feynman-Hellman theorem is used, which states how the eigenvalue λ corresponding to a normalized left (or right) eigenstate $\langle B|$ (or $|A\rangle$) of an operator \hat{H} changes upon parameter variation:

$$\partial_T \lambda = \partial_T \langle B| \hat{H} |A\rangle = \langle B| \partial_T \hat{H} |A\rangle. \quad (10)$$

In the present context, the non-Hermitian version of this lemma will be applied to the translational Goldstone mode (GM) $\mathbf{V}_+ = -\frac{1}{2}(\partial_x \mathbf{u}_0 - i\partial_y \mathbf{u}_0)$ and its associated response function (RF) \mathbf{W}^+ . These modes are the right and left eigenstates to $\hat{\mathbf{L}}_0 = \mathbf{D}\Delta + \omega_0\partial_\theta + \mathbf{f}(\mathbf{u}_0)$, associated to Eq. (1). The growth of small perturbations with wave number k_z will evolve as $\partial_t \hat{\mathbf{u}} = \hat{\mathbf{L}}\hat{\mathbf{u}}$, with $\hat{\mathbf{L}} = \hat{\mathbf{L}}_0 - k_z^2 \mathbf{D}$, as noted in [4]. Next, the eigenfunction $|\mathbf{V}_+\rangle$ to $\hat{\mathbf{L}}$ is expanded as

$$\lambda_+ = i\omega_0 - \gamma k_z^2 - g k_z^4 + \mathcal{O}(k_z^6), \quad (11)$$

with yet unknown complex coefficients $\gamma = \gamma_1 + i\gamma_2$, $g = g_1 + ig_2$. Calling $k_z^2 = T$, we will be looking for $\partial_T \lambda_+$ and $\partial_T^2 \lambda_+$, evaluated at $T = 0$. From Eq. (10) follows

$$\partial_T \lambda_+ = \langle \mathbf{W}^+ | \partial_T \hat{\mathbf{L}} | \mathbf{V}_+ \rangle = -\langle \mathbf{W}^+ | \mathbf{D} | \mathbf{V}_+ \rangle, \quad (12)$$

confirming the well-known expression for the filament tension coefficient, i.e. $\gamma = \gamma_1 + i\gamma_2 = \langle \mathbf{W}^+ | \mathbf{D} | \mathbf{V}_+ \rangle|_{k_z=0}$ [5-7]. In the next order, it holds that

$$\frac{1}{2} \partial_T^2 \lambda_1 = -\frac{1}{2} (\langle \partial_T \mathbf{W}^+ | \mathbf{D} | \mathbf{V}_+ \rangle + \langle \mathbf{W}^+ | \mathbf{D} | \partial_T \mathbf{V}_+ \rangle) \quad (13)$$

The derivative of the eigenfunctions can be evaluated by deriving $\hat{\mathbf{L}} |\mathbf{V}_+\rangle = \lambda_+ |\mathbf{V}_+\rangle$ with respect to T , delivering $(\hat{\mathbf{L}} - \lambda_+) |\partial_T \mathbf{V}_+\rangle = (\mathbf{D} - \gamma) |\mathbf{V}_+\rangle$. For $T = 0$, one finds

$$|\partial_T \mathbf{V}_+\rangle = (\hat{\mathbf{L}} - i\omega_0)^{-1} (\mathbf{D} - \gamma) |\mathbf{V}_+\rangle + a |\mathbf{V}_+\rangle \quad (14a)$$

$$\langle \partial_T \mathbf{W}^+ | = \langle \mathbf{W}_+ | (\mathbf{D} - \gamma) (\hat{\mathbf{L}} - i\omega_0)^{-1} - a \langle \mathbf{W}^+ | \quad (14b)$$

Substitution in Eq. (13) then delivers

$$\frac{1}{2} \partial_T^2 \lambda_1 = -\frac{1}{2} \left(\langle \mathbf{W}^+ | (\mathbf{D} - \gamma) (\hat{\mathbf{L}} - i\omega_0)^{-1} \mathbf{D} | \mathbf{V}_+ \rangle + \langle \mathbf{W}^+ | \mathbf{D} (\hat{\mathbf{L}} - i\omega_0)^{-1} (\mathbf{D} - \gamma) | \mathbf{V}_+ \rangle \right), \quad (15)$$

which can be symmetrized using $(\mathbf{D} - \gamma) |\mathbf{V}_+\rangle = \hat{\mathbf{\Pi}} \mathbf{D} |\mathbf{V}_+\rangle$ and $\langle \mathbf{W}^+ | (\mathbf{D} - \gamma) = \langle \mathbf{W}^+ | \mathbf{D} \hat{\mathbf{\Pi}}$, where $\hat{\mathbf{\Pi}} = (1 - |\mathbf{V}_+\rangle \langle \mathbf{W}^+ |)$ is a projection operator which commutes with $\hat{\mathbf{L}}$. Thus follows

$$g_1 + ig_2 = -\frac{1}{2} \partial_T^2 \lambda_1 = \langle \mathbf{W}^+ | \mathbf{D} (\hat{\mathbf{L}} - i\omega_0)^{-1} \hat{\mathbf{\Pi}} \mathbf{D} | \mathbf{V}_+ \rangle \quad (16)$$

Eq. (11) subsequently implies that systems with small, negative γ_1 can nevertheless be stable if all perturbation modes compatible with the boundary conditions satisfy $\text{Re}(\lambda_+) < 0$, i.e. $-\gamma_1 - g_1 k_z^2 < 0$. This can be the case when $g_1 > 0$, which will be assumed henceforth. For a straight filament between parallel impermeable boundaries of spacing L_z , k_z takes discrete values $n \frac{\pi}{L_z}$, $n \in N$, whence the straight filament remains stable if only

$$L_z < L_* = \frac{\pi}{k_*} = \pi(-g_1/\gamma_1)^{1/2} \quad (17)$$

The imaginary part of $\lambda_+ - i\omega_0$ represents the precession frequency of the buckled filament; it is given by $\Omega(k_z) = k_z^2(-\gamma_2 - g_2 k_z^2)$. At the instability threshold, it equals

$$\Omega_* = \gamma_1(\gamma_1 g_2 - \gamma_2 g_1)/g_1^2. \quad (18)$$

The equilibrium amplitude of buckled filaments can be derived from a filament equation of motion that takes into account the effects cubic in filament curvature effects; its detailed proof will be published elsewhere.

Computations required by the theory

Computations of spiral wave solutions \mathbf{U} , its angular velocity ω_0 , and their translational eigenmodes \mathbf{V}_+ and \mathbf{W}^+ was by `dxspiral` suite [8] based on the method described in [9], which depends on three discretization parameters: the disk radius ρ_{\max} , radial resolution N_ρ and angular resolution N_θ . For the eigenvalue problems, we used straight shift-invert Arnoldi iterations without Cayley transform, and Krylov dimensionality of 10. The list of computed quantities used in previous publications [9, 10] had to be extended to compute $g_1 + ig_2$, which involved computing of quasi-inverse $|\mathbf{a}\rangle \mapsto |\mathbf{b}\rangle$,

$$|\mathbf{b}\rangle = \hat{\mathbf{L}}' \hat{\mathbf{\Pi}} |\mathbf{a}\rangle$$

where $\hat{\mathbf{L}}'$ is the inverse

$$\hat{\mathbf{L}}' = (\hat{\mathbf{L}} - i\omega_0)^{-1},$$

in the subspace orthogonal to \mathbf{V}_+ , and $\hat{\mathbf{\Pi}}$ is the projection operator to that subspace,

$$\hat{\mathbf{\Pi}} = \mathbf{1} - |\mathbf{V}_+\rangle \langle \mathbf{W}^+ |.$$

Although exact $\hat{\mathbf{L}}'$ is not defined in the whole space, its numerical implementation is defined, but extremely ill-posed (condition number is the higher, the more accurate is the solution of the eigenvalue problem for \mathbf{V}_+), so this computation presented some challenge. To achieve satisfactory results, we did the following.

- We applied the projection operator before and after the inverse, each several times,

$$|\mathbf{b}\rangle = \hat{\mathbf{\Pi}}^k \hat{\mathbf{L}}' \hat{\mathbf{\Pi}}^m |\mathbf{a}\rangle$$

where k and m were taken as large as to ensure that further applications of $\hat{\mathbf{\Pi}}$ did not change the results any more at a given floating point precision (we used 8-byte arithmetics). Obviously, the exact $\hat{\mathbf{\Pi}}$ and $\hat{\mathbf{L}}'$ commute, so multiple applications of $\hat{\mathbf{\Pi}}$ would not change the result “in the ideal world”, and in the real computations they minimized the impact of the round-off errors and the magnifying effect of the ill-posed $\hat{\mathbf{L}}'$.

- Apart from straight application of the inverse $\hat{\mathbf{L}}'$ through LU decomposition, we also tried iterative application of the same, a version of GMRES method and Tikhonov regularization.

The quality of the quasi-inverse was assessed by normalized residual

$$\| |\mathbf{a}\rangle - \hat{\mathbf{L}} |\mathbf{b}\rangle \| / \| |\mathbf{a}\rangle \|,$$

where the norm is in l_2 . We found that with multiple application of $\hat{\mathbf{\Pi}}$, the simplest method gives a satisfactory quality (normalized residual of the order of 10^{-2} or less) which is not easily improved with the other, more time-consuming methods.

The continuation problem (8) was done at the same discretization as the unperturbed spiral wave solution \mathbf{U} and the eigenmodes \mathbf{V}_+ and \mathbf{W}^+ of the asymptotic theory.

The choices of discretization parameters used for specific results are summarized in Table II.

TABLE II: Discretization parameters for `dxspiral` calculations.

Figure	ρ_{\max}	N_θ	N_ρ
2(b)	16	320	96
3(b)	25	1000	64
3(d)	16	1280	64

-
- [1] D. Barkley and M. Dowle, *EZ-SCROLL: A code for simulating scroll waves*, http://www.warwick.ac.uk/~masax/Software/ez_software.html (2007).
- [2] P. L. T. Brian, *A. I. Ch. E. Journal* **7**, 367 (1961).
- [3] B. Carnahan, H. A. Luther, and J. O. Wilkes, *Applied numerical methods* (John Wiley & Sons, Inc., New York, 1969).
- [4] H. Henry and V. Hakim, *Phys. Rev. E* **65**, 046235 (2002).
- [5] J. Keener, *Physica D* **31**, 269 (1988).
- [6] V. N. Biktashev, A. V. Holden, and H. Zhang, *Phil. Trans. Roy. Soc. Lond. ser. A* **347**, 611 (1994).
- [7] H. Verschelde, H. Dierckx, and O. Bernus, *Phys. Rev. Lett.* **99**, 168104 (2007).
- [8] D. Barkley, V. N. Biktashev, I. V. Biktasheva, G. V. Bordyugov, and A. J. Foulkes, *DXSpiral: a code for studying spiral waves on a disk*, <http://www.csc.liv.ac.uk/~ivb/software/DXSpiral.html>.
- [9] I. V. Biktasheva, D. Barkley, V. N. Biktashev, G. V. Bordyugov, and A. J. Foulkes, *Phys. Rev. E* **79**, 056702 (2009).
- [10] I. V. Biktasheva, D. Barkley, V. N. Biktashev, and A. J. Foulkes, *Phys. Rev. E* **81**, 066202 (2010).